STEM CELLS®

EMBRYONIC STEM CELLS/INDUCED PLURIPOTENT STEM CELLS

Telomere Length Defines the Cardiomyocyte Differentiation Potency of Mouse Induced Pluripotent Stem Cells

TANIA AGUADO,[a] FRANCISCO J. GUTIÉRREZ,[b] ESTHER AIX,[a] RALPH P. SCHNEIDER,[c] GIOVANNA GIOVINAZZO,[b] MARÍA A. BLASCO,[c] IGNACIO FLORES[a]

Key Words. Induced pluripotent stem cells • Telomere length • Cardiomyocytes • Extracellular matrix • Ascorbic acid

[a]Regeneration and Aging Group, [b]Pluripotent Cell Technology Unit, Centro Nacional de Investigaciones Cardiovasculares (CNIC-ISCIII), Madrid, Spain; [c]Telomeres and Telomerase Group, Molecular Oncology Program, Spanish National Cancer Research Centre (CNIO), Madrid, Spain

Correspondence: Ignacio Flores, Dr., Fundacion Centro Nacional de Investigaciones Cardiovasculares Carlos III, Madrid, Spain. Telephone: (+34) 914531200; Fax: (+34) 91 4531245; e-mail: iflores@cnic.es

Received March 2, 2016; accepted for publication August 16, 2016; first published online in STEM CELLS *EXPRESS* September 26, 2016.

1066-5099/2016/$30.00/0

http://dx.doi.org/10.1002/stem.2497

ABSTRACT

Induced pluripotent stem cells (iPSCs) can be differentiated *in vitro* and *in vivo* to all cardiovascular lineages and are therefore a promising cell source for cardiac regenerative therapy. However, iPSC lines do not all differentiate into cardiomyocytes (CMs) with the same efficiency. Here, we show that telomerase-competent iPSCs with relatively long telomeres and high expression of the shelterin-complex protein TRF1 (iPSC^{highT}) differentiate sooner and more efficiently into CMs than those with relatively short telomeres and low TRF1 expression (iPSC^{lowT}). Ascorbic acid, an enhancer of cardiomyocyte differentiation, further increases the cardiomyocyte yield from iPSC^{highT} but does not rescue the cardiomyogenic potential of iPSC^{lowT}. Interestingly, although iPSCs^{lowT} differentiate very poorly to the mesoderm and endoderm lineages, they differentiate very efficiently to the ectoderm lineage, indicating that cell fate can be determined by in vitro selection of iPSCs with different telomere content. Our findings highlight the importance of selecting iPSCs with ample telomere reserves in order to generate high numbers of CMs in a fast, reliable, and efficient way. STEM CELLS *2017;35:362–373*

SIGNIFICANCE STATEMENT

After a heart attack, a significant proportion of cardiomyocytes (CMs) are lost. Two main strategies are under investigation to replace such a large number of CMs: the induction of proliferation of endogenous cardiac cells and the engraftment of exogenous CMs into the heart. A major source for exogenous CMs in cell replacement therapy is iPSCs. However not all iPSC lines differentiate into CMs with the same efficiency and not all have the same telomere length. Our results indicate that the differentiation efficiency of iPSCs into CMs correlates positively with telomere length. Selection of iPSC lines with ample telomere reserves thus presents an attractive strategy to generate high numbers of CMs in a fast, reliable, and efficient way.

INTRODUCTION

Cardiomyopathies and acute myocardial infarction constitute the leading cause of death worldwide [1]. Although extensive efforts have been made to develop new therapies to treat patients with heart disease, the ability to repair a damaged heart remains elusive [2, 3]. Cell-based regenerative therapy has emerged as a promising treatment for heart failure, prompting research to identify the best cell candidate that could lead to recovery of heart function. The heart has been grafted with various cell types at different developmental stages, including embryonic, foetal, and adult cells [4]; however, their reparative effect has been partial and variable [5, 6]. Further studies are therefore needed to identify the cell sub-type with the highest reparative potential.

Induced pluripotent stem cells (iPSCs) can be differentiated in vitro and in vivo to all cardiovascular lineages [7–10]. However, heart recovery rates after injection of iPSC-derivatives into infarcted hearts are unsatisfactory [10–12]. A potential limitation of iPSC-based regenerative therapy is the large number of cardiac cells that need to be replaced after a heart attack [13]. Not all iPSC lines differentiate into the cardiac lineage with the same efficiency [14], and it is therefore desirable to select those that generate the largest number of cardiac cells. The varied propensity of iPSCs to differentiate into cardiac lineages

might reflect inherent iPSC molecular heterogeneity [15]. The specific molecular factors that contribute to differentiation-fate decisions are only now beginning to be defined.

Telomeres are DNA–protein complexes that protect the ends of chromosomes from DNA repair and degradation [16]. Telomerase activity is higher in iPSCs than in their parental somatic cells [17, 18], reflecting the importance of telomere elongation during somatic cell reprogramming for iPSC generation and functionality [17, 19–22]. Different iPSC lines and different cells of the same iPSC line vary in the length of their telomeres [19]. However, it remains unclear whether telomere length is a suitable indicator of iPSC cardiac differentiation efficiency.

In this study, we demonstrate that telomere length defines the potential of iPSCs to differentiate toward a cardiac fate. iPSCs with relatively long telomeres tend to differentiate to the mesoderm and endoderm lineages, in part by building a suitable microenvironment that facilitates first the generation of cardiac progenitor cells and subsequently their differentiation into contracting cardiomyocytes (CMs). These results indicate the value of checking iPSC telomere length before generating CMs in order to select those ones with ample telomere reserves.

Materials and Methods

iPSC Culture and Differentiation

iPSCs were maintained in the undifferentiated state by culturing on feeder layers of mytomicin-inactivated primary mouse embryo fibroblasts (MEFs). Cultures were maintained in proliferation medium, consisting of high-glucose DMEM-GlutaMAX medium (Invitrogen) supplemented with 15% high quality fetal bovine serum (FBS), 0.1 mM non-essential amino acids (Invitrogen), 0.1 mM β-mercaptoethanol (Sigma) and leukemia inhibitory factor (LIF). Medium was changed daily, and cells were passaged every 2 days.

Differentiation of iPSCs was initiated by the hanging-drop method [23]. Briefly, iPSCs were grown in iPSC-differentiation medium (proliferation medium without LIF) supplemented with 20% FBS and suspended in hanging drops at 1000 cells per 20 μl drop. Embryoid bodies (EBs) were collected on day 2 and differentiated further on uncoated dishes in differentiation medium with 15% FBS. On day 5, EBs destined for adherent culture were seeded one per well onto p96 well dishes coated with gelatin (0.1%), type IV collagen (10 μg/cm^2; C6745, Sigma-Aldrich, St. Louis, MO), or Matrigel (8.3 μg/cm^2; 354277, Corning). Alternatively, EBs were maintained in floating culture for extracellular matrix (ECM) and outer-layer staining, cystic EBs analysis, and chimeric EBs experiments. Samples were collected at days 3, 5, 7, 10, and 15 after initiation of differentiation. Beating colonies on 96-well plates were counted and the percentage of beating EBs calculated. At least 100 EBs per time point and condition were evaluated in each experiment. For experiments with ascorbic acid (AA), 50 μg/ml of AA (Sigma) was added beginning at day 2 of differentiation and continuing until the final day of the experiment [24]. In all differentiation experiments medium was renewed every 2–3 days.

For chimeric experiments, 1×10^5 feeder-free iPSCs were transduced in the presence of 8 μg/ml of Polybrene with a lentivirus supernatant (MOI:5) carrying the tdTomato reporter gene (PGK-tdTomato, produced by the CNIC Pluripotent Cell Technology Unit). Transduction was carried out for 12 hours at 37°C in 5% CO_2. At 5 days after transduction, tdTomato-positive cells (red-orange fluorescent protein) were sorted on a flow-assisted cell sorting (FACS) Aria II cell sorter (BD Biosciences) and grown in proliferation medium at low density (500 cells/p35) on feeder layers. Upon appearance of ESC-like colonies, single colonies were picked based on morphology and tdTomato expression, and expanded on inactivated MEFs.

Flow-Assisted Cell Sorting (FACS)

G1 eGFP-TRF1 iPSCs were dissociated to single cells with 0.025% trypsin (Invitrogen) and depleted of feeder cells by culturing for 45 minutes in iPSC medium at 37°C and 5% CO_2. Floating iPSCs were incubated for 30 minutes at 37°C with 10 mg/ml Hoechst33342 (Sigma) and 50 μM verapamil (Sigma) at a concentration of 1×10^6 cells per ml. G1 cells were FACS sorted on an FACS Aria II (BD Biosciences) according to eGFP relative fluorescence intensity (10% fractions of eGFP^{low} and eGFP^{high}). TO-PRO-3 was used to exclude dead cells.

Flow Cytometry

Sorted iPSCs or trypsin-dissociated EBs where fixed and permeabilized with ice-cold 90% methanol. Cells were stained with goat anti-GFP (Acris), rabbit anti-Nanog (Millipore), or mouse anti-Oct3/4 (Santa Cruz), followed by secondary antibodies as appropriate: anti-goat (Alexa 488, Invitrogen), anti-rabbit (Cy5 conjutated; Jackson laboratorys), or anti-mouse IgG2a (Alexa 488, Invitrogen). At least 5×10^5 cells were incubated with primary antibodies for 60 minutes at 4°C. In each measurement, at least 1×10^4 events were analyzed in a FACS CantoII or LSRFortessa machine (BD Biosciences), and data were analyzed using FACSDiva software (BD Biosciences). For flow cytometry analysis three independent experiments were performed in triplicate.

Histology and Immunostaining

iPSCs or differentiating EBs cultured on gelatin coated coverslips for the indicated times were fixed for 10 minutes in 4% paraformaldehyde, 5% sucrose in phosphate buffered saline (PBS), followed by three washes in PBS. Floating EBs were briefly rinsed in PBS and subsequently fixed in 4% paraformaldehyde for 30 minutes (EBs from day 2 and day 5) or overnight at 4°C (EBs from day 10 or 15). For immunofluorescence analysis, PFA-fixed EBs were incubated overnight in 30% sucrose/PBS at 4°C, and then included in gelatin/sucrose and frozen for cryostat sectioning. Fixed iPSCs, plated EBs, and cryosectioned EBs were incubated at room temperature with 0.25% Triton X-100 in PBS for 30 minutes, followed by incubation in 5% FBS, PBS for 1 hour and then stained in PBS containing 0.025% Triton X-100 and 1% FBS. Incubation with primary antibody was carried out overnight at 4°C; antibodies are indicated below. Appropriate Alexa secondary antibodies (Invitrogen) were diluted 1:1000 in PBS and incubations were carried out for 1h at RT. Nuclei were counterstained with DAPI (4′,6-diamidino-2-phenylindole; 1:1000 dilution of 5 mg/ml stock), and stained samples were mounted in Vectashield (Vector labs).

For histological analysis, EBs were dehydrated and embedded in paraffin. Paraffin-rehydrated sections (5 μm) were

stained with hematoxylin and eosin (H&E) using a standard protocol. Sections were examined for pH3 expression by immunohistochemial staining with a specific primary antibody, and positive cells were visualized using 3,3-diaminobenzidine tetrahydrochloride plus (DAB+) as chromogen. The primary antibodies used in this study were mouse anti-α-actinin (1:200, Sigma), rabbit anti-α-1-fetoprotein (1:500, Dako), mouse anti-Cardiac troponinT (1:200, Hybridoma Bank, clone CT3), rabbit anti-Collagen IV (1:200, Millipore), rabbit anti-Dsred (1:500, Clontech), goat anti-GFP (1:100, Acris), mouse anti-Myosin heavy chain (1:20, Hybridoma Bank MF20), rabbit anti-Nanog (1:200, Millipore), rabbit anti-Nkx2.5 (1:50, Santa Cruz), mouse anti-Oct3/4 (1:200, Santa Cruz), rabbit anti-phospho-Histone H3 (Ser10) (1:200, Millipore), goat anti-Sox17 (1:500, Dako), rabbit anti-TroponinI (1:200, Abcam), and rabbit anti-Zscan4 (1:200, Millipore).

Image Analysis

Z-stack images of fluorescence stainings were acquired with a Leica TCS SP-5 confocal microscope, and maximum projections were generated with LAS AF software (Leica). H&E and pH3 stained sections were mounted, and bright-field images were captured with a Nikon Eclipse 90i microscope. Images were prepared for figures using Adobe Photoshop CS5.1. The area of α-actinin immunostaining in plated EBs (1 EB/well) was quantified using five mosaic reconstruction images of whole plated EBs, and the area of staining was calculated as a percentage of the total possible area (DAPI-positive area) using ImageJ software (National Institutes of Health, Bethesda, MA, USA). Cells positive for specific markers were quantified relative to the total cell number (DAPI-positive). At least 20 EBs were analyzed per condition. For iPSC staining, positive cells were quantified in ≥10 randomly selected fields after DAPI counterstaining. For EB size analysis, at least 100 EB diameters were measured for each condition and time point using ImageJ. For quantification of type IV collagen, maximum projection Z-stacks of cryosectioned EBs were reconstructed, and the collagen IV signal was analyzed using the Image J area integrated density measurement tool. Signals were subjected to threshold processing. For imaging quantification, at least three independent experiments were performed for each condition.

Telomere Quantitative Fluorescence In Situ Hybridization (QFISH)

Telomere length in iPSCs was assessed by QFISH. Briefly, 2×10^4 sorted iPSCs in 200 μl PBS were attached to glass slides by cytospin. After air-drying, slides were treated with a 3:1 mix of methanol and ethanoic acid for 30 minutes. Telomere FISH was performed and quantified as described [25]. DAPI and telomere fluorescence signals (cy3) were acquired into separate channels with a Leica SP5 confocal microscope fitted with a ×40 objective. For image quantification, maximum projections of 5 × 5 mosaic images were generated (15 sections at 1.0 μm steps), and images were quantified using the Metamorph platform (Molecular Devices) [25]. At least three independent experiments were carried out for each condition.

Reverse Transcription and Quantitative PCR

Total RNA was isolated using the Direct-zol RNA MiniPrep Kit (ZymoResearch). RNA (500 ng) was retrotranscribed using the High Capacity RNA-to-cDNA Kit (Life Technologies). Semi-quantitative PCR was performed with GoTaq mastermix. SYBR Green real-time PCR reactions (Life technologies) were performed in triplicate using an ABI PRISM 7900HT FAST Real-Time PCR System and 40 cycles of amplification (95°C 10 seconds; 60°C 30 seconds; 72°C 30 seconds). The expression level of each gene was determined by the relative standard curve method, performed by making serial dilutions of iPSC or mouse heart mRNA. All values were normalized to EEF1 and GusB as endogenous controls. Results are shown as fold change over EFF1 levels. Each experiment was performed independently at least three times. Primer sequences for target genes were obtained from the Universal ProbeLibrary Assay Design Center (https://qpcr.probefinder.com/organism.jsp). At least three independent experiments were carried out for each condition.

Protein Extraction and Immunoblot

Protein extracts were prepared with Laemmli buffer [26]. Total proteins (30 μg) were separated by SDS-PAGE and transferred to polyvinylidene difluoride membranes. Antibody incubations and washes were carried out according to standard procedures. After incubation with horseradish peroxidase-conjugated secondary antibody (Dako), signal was detected using the ECL system (Amersham). The following primary antibodies were used: mouse anti-α-actinin (Sigma), mouse anti-α tubulin and anti-β-actin (Sigma). Densitometric analysis was performed using Quantity One. At least three independent experiments were carried out for each condition.

Statistics

Statistical comparisons were made using GraphPad Prism 5. Data are presented as means ± SEM or ± SD, as indicated in each figure. Significance of differences were calculated by *t* test for comparisons between two groups, ANOVA with Bonferroni post-test for multiple pair-wise comparisons, and Mann–Whitney test or Kruskal–Wallis test for QFISH analysis.

Results

Robust Cardiomyocyte Differentiation of iPSCs with Relatively Long Telomeres

To investigate whether the differentiation efficiency of iPSCs into CMs is dependent on telomere length, we separated iPSCs into two subpopulations according to telomere length. We used eGFP-TRF1 iPSCs, a system that allows the separation of iPSCs according to the expression levels of telomere-repeat-binding factor 1 (TRF1) and telomere content [22]. To avoid possible cell-cycle–related differences in telomere number, we analyzed only cells in G1. The 10% fraction of G1 eGFP-TRF1 iPSCs with the highest GFP intensity ($iPSC^{highT}$) had elevated *Trf1* expression levels and relatively long telomeres, whereas the 10% G1 eGFP-TRF1 iPSCs fraction with the lowest GFP intensity ($iPSC^{lowT}$) had lower *Trf1* expression levels and relatively short telomeres (Supporting Information Fig. S1). Spontaneous cardiomyocyte differentiation was induced in unseparated G1 cells (control), $iPSC^{highT}$, and $iPSC^{lowT}$ by LIF withdrawal [23] (Fig. 1A). When cultured in the absence of LIF, iPSCs spontaneously aggregate in 3D spheroids called EBs, some of which progressively begin to beat. Analysis of the number of EBs with beating areas and the time of beating

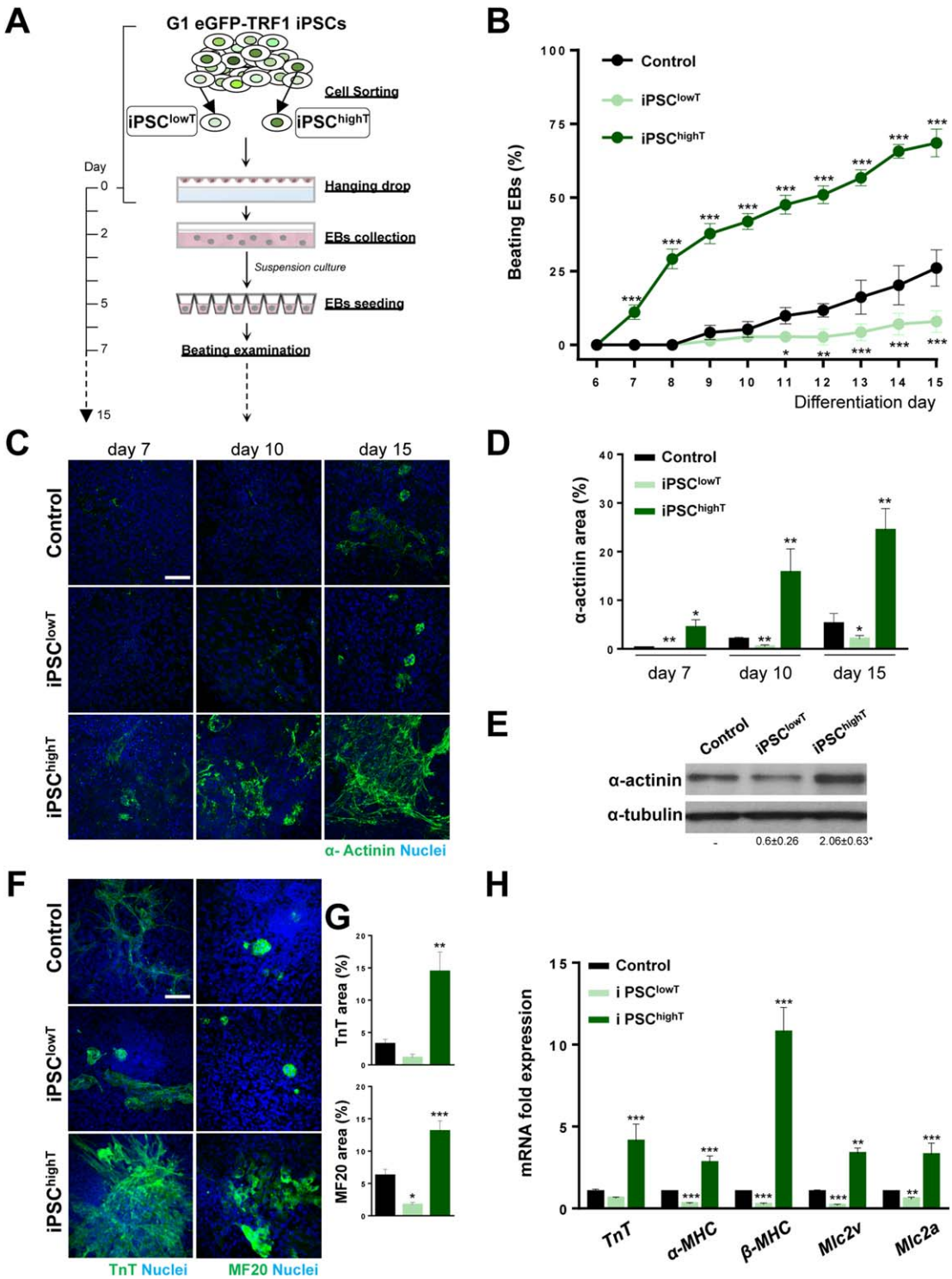

Figure 1. Selection of iPSCs with relatively long telomeres improves spontaneous cardiomyocyte differentiation efficiency**. (A)**: Protocol used to generate CMs from selected iPSC populations. Control: G1 iPSCs; iPSC^{lowT}: G1 iPSCs with relatively short telomeres; iPSC^{highT}: G1 iPSCs with relatively long telomeres. **(B)**: Percentages of beating iPSC-derived EBs from day 6 through day 15. **(C)**: Representative images showing α-actinin expression levels during iPSC differentiation into CMs. Scale bar, 80 μm. Nuclei were counterstained with DAPI. **(D)**: Quantification of α-actinin area in iPSC-derived EBs differentiating into CMs. **(E)**: α-actinin expression measured by western blot on differentiation day 15. α–tubulin was used as loading control. Numbers represent densitometric fold change relative to control. **(F)**: Representative images showing troponin T (TnT) and sarcomere myosin (MF20) expression on day 15. Scale bar, 80 μm. Nuclei were counterstained with DAPI. **(G)**: Quantification of TnT and MF20 area on differentiation day 15. **(H)**: Expression of CM-associated genes analyzed by qRT-PCR on differentiation day 10. All bars and values show means ± SEM. All experiments, $n \geq 4$. *, $p < .05$; **, $p < .01$; ***, $p < .001$ versus control. Abbreviations: CMs, cardiomyocytes; EBs, embryoid bodies; iPSCs, induced pluripotent stem cells.

onset showed that iPSC^{highT}-derived EBs began to beat earlier and in greater numbers than those derived from iPSC^{lowT} or controls (Fig. 1B). After 15 days in culture, iPSC^{highT} differentiated into beating EBs 7.5 times more than iPSC^{lowT} cells and 2.7 times more than control cells, suggesting that selection of iPSC^{highT} from the iPSC pool markedly improves differentiation efficiency toward the CM lineage (Fig. 1B).

To verify that the beating cells were mature CMs, we examined the emergence of CM markers by immunofluorescence. Under differentiation conditions, iPSC^{highT} showed progressive expression of the CM sarcomere protein α-actinin, whereas expression in iPSC^{lowT} remained very low even after 15 days (Fig. 1C, 1D). Differential expression of α-actinin on day 15 between iPSC^{highT}- and iPSC^{lowT}-derived EBs was corroborated by western blot (Fig. 1E). Immunofluorescence on day 15 for two additional CM markers, sarcomere myosin (MF20) and troponin T (TnT), further confirmed that iPSC^{highT} cells differentiate into mature CMs more efficiently than iPSC^{lowT} or control iPSCs (Fig. 1F, 1G). Consistent with the higher protein expression of CM markers, iPSC^{highT}-derived EBs had significantly higher mRNA expression of the CM genes *TnT, alpha-myosin heavy chain* (*α–MHC*), *beta-myosin heavy chain* (*β-MHC)*, *myosin light chain 2 ventricular transcript* (*Mlc2v*), and *myosin light chain 2 atrial transcript* (*Mlc2a*), reflecting efficient maturation into ventricular and atrial CMs (Fig. 1H). Taken together, these data indicate that selection of iPSCs with relatively long telomeres before differentiation strongly increases the number of differentiated mature CMs and conversely that iPSCs with relatively short telomeres have a deficient differentiation toward the CM lineage.

Telomere Length Defines the Cardiomyocyte Differentiation of iPSCs from Their Initial Stages

The generation of mature CMs from iPSCs after LIF removal follows a series of consecutive differentiation stages marked by the sequential expression of genes associated with pluripotency, early mesoderm, cardiac progenitors, and differentiated CMs [27, 28]. To determine the differentiation stage at which conversion of iPSC^{highT} into CMs was facilitated and conversion of iPSC^{lowT} obstructed, we monitored mRNA expression of genes associated with pluripotency, early mesoderm, cardiac progenitors, and CMs over the differentiation time course. We also monitored expression of the main DNA methyltransferases in undifferentiated iPSCs because DNA methylation is fundamental to the correct establishment and maintenance of the pluripotent state [29] and de novo methyltransferase expression is downregulated in embryonic stem cells (ESC) with critically short telomeres [21]. Interestingly, iPSC^{lowT} had lower mRNA levels of *Dnmt3b* than control iPSCs, whereas expression of *Dnmt3b* and *Dnmt1* in iPSC^{highT} was higher (Supporting Information Fig. S2A); however, these changes were modest compared with those observed in ESC with critically short telomeres [21]. These results indicate that iPSC subpopulations differing in telomere content also differ in expression of DNA methyltransferases, which could affect their ability to initiate differentiation. Subsequent qRT-PCR analysis revealed that initial iPSC differentiation was marked by decreases in the pluripotency markers *Oct3/4* and *Nanog*, consistent with the activation of differentiation transcriptional programs in control iPSCs, iPSC^{highT}, and iPSC^{lowT}. However, compared with controls, levels of *Oct3/4* and *Nanog* at days 3 and 5 after LIF removal were significantly lower in iPSC^{highT}-derived EBs and significantly higher in iPSC^{lowT}-derived EBs (Fig. 2A). The correlation between telomere content and low *Oct3/4* and *Nanog* mRNA levels was also observed for protein expression assessed by flow cytometry and immunofluorescence (Fig. 2B, 2C). The downregulation of pluripotency genes in day-3 iPSC^{highT}-derived EBs was accompanied by marked upregulation of the early-mesodermal genes *Brachyury, Mesp1*, and *Dkk1* (Fig. 2D). Interestingly, despite the low levels of these genes in undifferentiated iPSCs, iPSC^{highT} expressed higher levels of *Dkk1* than iPSC^{lowT} before LIF removal (Supporting Information Fig. S2B). Similar to the expression of early-mesodermal genes, expression of the cardiac-progenitor-specific transcription factors *Tbx5*, *Gata4*, and *Nkx2.5* in iPSC^{highT}-derived EBs on day 7 was double that in control EBs (Fig. 2E). Immunofluorescence analysis confirmed the robust increase in the expression of Nkx2.5 in differentiating iPSC^{highT} on day 7 (Fig. 2F). Conversely, expression of these early mesoderm and cardiac progenitor genes was impaired in iPSC^{lowT} during the spontaneous differentiation process (Fig. 2D-2F). The temporal patterns of gene expression associated with pluripotency, early mesoderm, cardiac progenitors, and differentiated CMs further indicated that iPSC^{highT} and iPSC^{lowT} differ in their ability to differentiate toward the cardiac lineage at a stage before the induction of mesoderm derivatives (Supporting Information Fig. S3A). Moreover, the expression levels of *Gfp* equalized in the three EB populations on day 2 of differentiation and those of *Trf1* and telomere lengths equalized on day 5 (Supporting Information Fig. S3B, S3C). These expression data reinforce the conclusion that telomere content defines iPSC fate decisions during the early stages of differentiation. Notably, *Trf1* downregulation during differentiation might be explained by the parallel reduction in Oct3/4, since this pluripotent factor binds to the TRF1 promoter, reducing its expression [22].

Embryoid Bodies Derived from iPSCs with Distinct Telomere Content Vary in Size, Cell Composition, and Number of Cysts

Previous reports indicate that the differentiation efficiency of mouse ESCs is influenced by EB size, with EBs of intermediate size showing the greatest differentiation potential [30]. We therefore analyzed the influence of iPSC telomere length on EB size. After 2 days of differentiation, iPSC^{highT}-derived EBs were larger than iPSC^{lowT}-derived or control EBs, and these size differences were increased further by day 5 (Fig. 3A, 3B). Immunofluorescence staining for the mitosis marker phospho–histone H3 (Ser10) (pH3) revealed an elevated proliferation capacity in iPSC^{highT}-derived EBs and a diminished capacity in iPSC^{lowT}-derived EBs (Fig. 3C, 3D), pointing to distinct proliferation rates as a likely contributor to the size difference between EBs with differing telomere content. However, significant differences in proliferation frequency were not observed between sorted iPSC^{highT} and iPSC^{lowT} growing in proliferation medium (containing LIF) (Supporting Information Fig. S4A, S4B). Therefore, initial telomere length appears to be important for iPSC propagation in differentiation conditions, but not for their propagation in proliferation conditions. Indeed, iPSC^{lowT} maintained in proliferation medium restored control eGFP levels over a few passages (Supporting Information Fig. S4C), resulting in a recovery in EB size (Supporting Information Fig. S4D) and beating efficiency (Supporting Information Fig. S4E).

In addition to cell proliferation, proper EB growth requires the generation of endodermal cells. qRT-PCR showed increased expression of early-endoderm specific markers in sorted iPSC^{highT} before LIF removal (Supporting Information Fig. S5A), suggesting that signaling cues responsible for

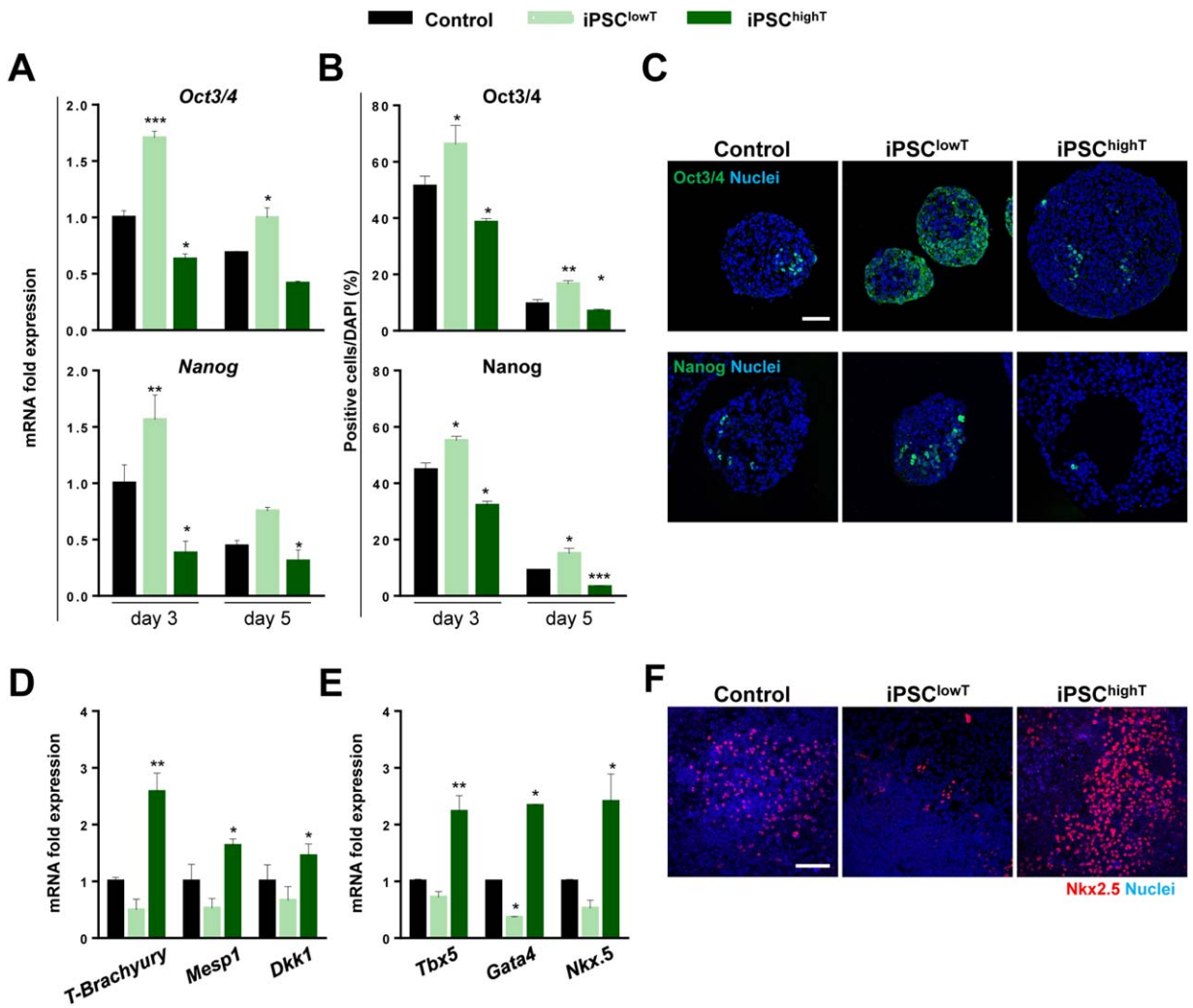

Figure 2. iPSC telomere length defines cell-fate decisions during early differentiation. **(A)**: qRT-PCR analysis of *Oct3/4* and *Nanog* gene expression levels during iPSC differentiation. **(B)**: Flow cytometry analysis of the percentage of iPSCs displaying detectable Oct3/4 or Nanog expression during iPSC differentiation. **(C)**: Representative immunohistochemistry images showing Oct3/4 and Nanog protein expression in cryosected day-5 EBs. Scale bar, 60 μm. **(D)**: qRT-PCR analysis of early mesodermal markers (*Brachyury, Mesp1, Dkk1*) in day-3 EBs. **(E)**: qRT-PCR analysis of cardiac progenitor transcripts (*Tbx5, Gata4, Nkx2-5*) in day-7 EBs. **(F)**: Representative immunohistochemistry images showing Nkx2.5 protein levels in day-7 EBs. Scale bar, 80 μm. All bars and values show means ± SEM. All experiments, $n \geq 4$. *, $p < .05$; **, $p < .01$; ***, $p < .001$ versus control. Abbreviations: EBs, embryoid bodies; iPSCs, induced pluripotent stem cells.

guiding early-endoderm development are enriched in iPSCs with relative long telomeres. To further assess the potency of iPSC^{highT} to differentiate into endoderm, we examined the formation of the outer endoderm layer, a structure with similarities to the extra-embryonic primitive endoderm that provides factors needed for the survival and differentiation of inner cells [31–33]. The expression levels of *Sox17* and *Afp,* two extra-embryonic endoderm markers [34–37], were notably higher in iPSC^{highT}-derived EBs than in control or iPSC^{lowT}-derived EBs (Fig. 3E). Immunofluorescence analysis confirmed high levels of Sox17 and Afp in the outer layer of iPSC^{highT}-derived EBs (Fig. 3F). In contrast, iPSC^{lowT}-derived EBs had low levels of Sox17 and Afp and did not express these endodermal markers in most outer layer cells (Fig. 3F). Telomere length thus determines the differentiation of primitive endoderm.

The outer endodermal EB cells secrete ECM components, forming a basement membrane (BM) that supplies survival factors to nearby EB cells [38–40] whereas EB cells far from the BM undergo apoptosis, which contributes to EB cavitation [31, 33, 41]. Before differentiation, iPSC^{highT} showed higher transcript expression than iPSC^{lowT} of the essential BM components *Col4a1*, *Col4a2*, *Lama1*, and *Lamb1* (Supporting Information Fig. S5B). To confirm the influence of iPSC telomere content on the degree of BM assembly in EBs, we determined the localization and expression levels of the ECM components fibronectin and collagen type IV [42]. iPSC^{highT}-derived EBs contained a well-structured BM characterized by abundant expression of collagen type IV (Fig. 4A, 4B; Supporting Information Fig. S6A, S6B) and fibronectin (Supporting Information Fig. S6C), consistent with the high endodermal marker expression in their outer layer. In contrast, iPSC^{lowT}-derived EBs showed sparse and disorganized expression of collagen type IV (Fig. 4A, 4B; Supporting Information Fig. S6A, S6B) and fibronectin (Supporting Information Fig. S6C), suggesting disrupted deposition in the EB discontinuous BM. We also found

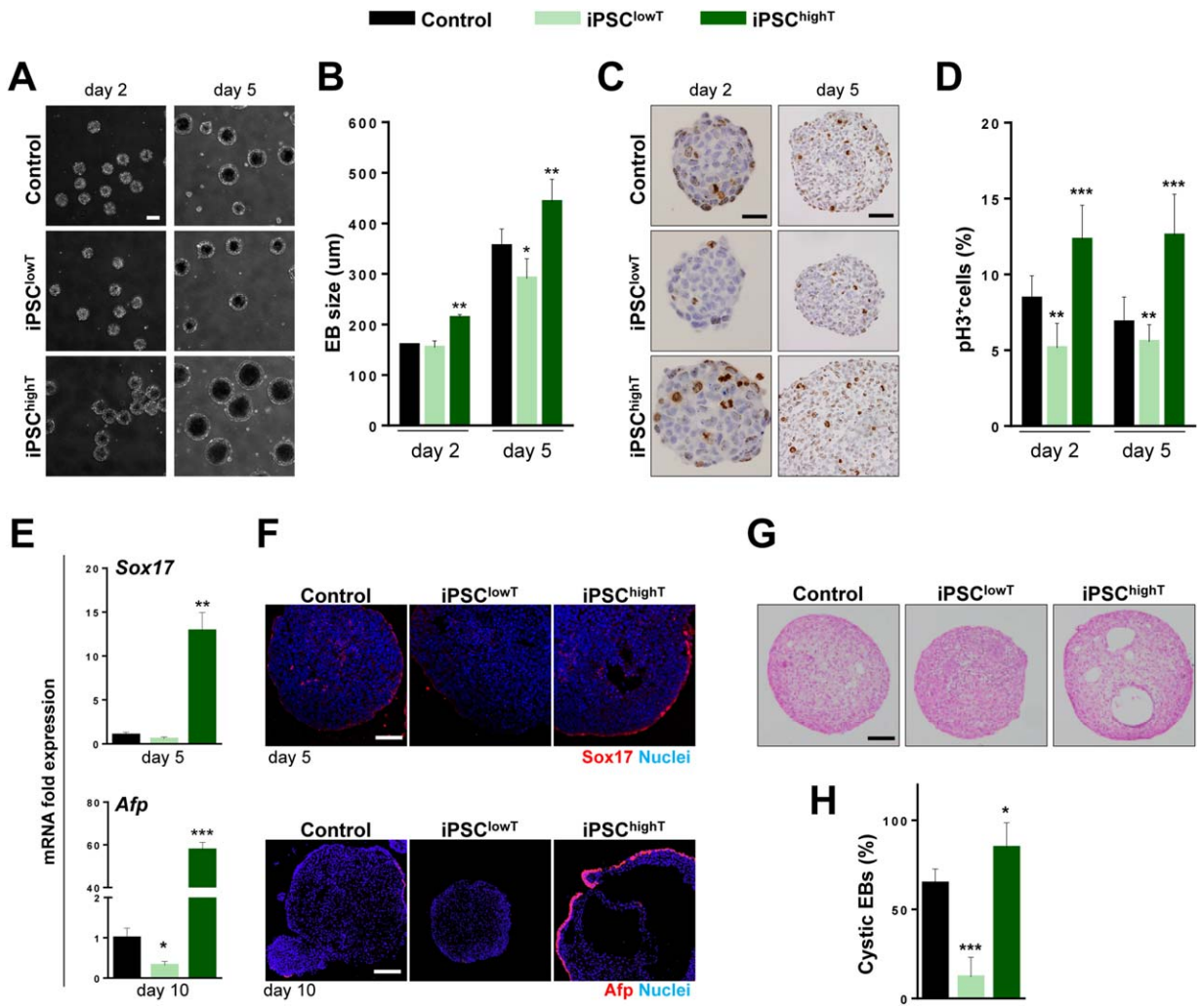

Figure 3. iPSCs with relatively long telomeres differentiate into bigger EBs covered by a properly formed outer endoderm layer. **(A)**: Phase contrast microscopy of EBs during the differentiation of iPSCs of differing telomere length. Scale bar, 200 μm. **(B)**: Quantification of EB diameters on day 2 and day 5 of iPSC differentiation. **(C)**: Representative pH3 immunostaining in day-2 and day-5 EBs. Scale bars, 35 μm on day 2; 80 μm on day 5. **(D)**: Quantification of pH3-positive cells on differentiation days 2 and 5. **(E)**: qRT-PCR analysis of the endoderm markers *Sox17* (day-5 EBs) and *Afp* (day-10 EBs). **(F)**: Representative immunostaining showing Sox17 and Afp protein levels and localization in day-5 and day-10 EBs. Scale bars, 70 μm and 200 μm. **(G)**: Hematoxylin and eosin stained histological sections of paraffin-embedded EBs on differentiation day 10. Scale bar, 200 μm. **(H)**: Percentage of embryonic bodies containing cysts. Bars and values show means ± SEM. *, $p < .05$; **, $p < .01$; ***, $p < .001$ versus control. Abbreviations: EBs, embryoid bodies; iPSCs, induced pluripotent stem cells.

that most iPSC^{highT}- and control-derived EBs formed cystic cavities (Fig. 3G, 3H), whereas iPSC^{lowT}-derived EBs mostly lacked cavities (Fig. 3G, 4A, and 4B), consistent with the contribution of a well-structured BM to cavity induction.

Ascorbic Acid Enhances Collagen Deposition and Cardiomyocyte Differentiation of iPSCs with Ample Telomere Reserves, but Not of Those with Low Telomere Content

AA increases the efficiency of iPSC differentiation into CMs by changing the ECM composition of EBs. Specifically, AA induces the expression of collagen [24, 43], an indispensable ECM and BM component. Expression analysis revealed that AA significantly increased *Col4a1* levels in EBs (Supporting Information Fig. S6B). Immunofluorescence analysis confirmed an AA-dependent increase in collagen IV protein, deposited just beneath the endoderm where the BM is located (Fig. 4A, 4B; Supporting Information S6B). Moreover, AA-induced collagen IV expression was not observed in iPSC^{lowT}-derived EBs (Fig.4A, 4B; Supporting Information Fig. S6A, S6B). AA-treated EBs also showed elevated fibronectin matrix deposition, with fibronectin expression highest in AA-treated iPSC^{highT}-derived EBs (Supporting Information Fig. S6C).

Previous studies indicated that AA-induced collagen expression enhances iPSC differentiation into CMs by supporting the expansion of cardiac progenitors [24]. iPSC^{highT}- and control-derived EBs both showed an AA-dependent increase in cardiac progenitor and CM marker gene expression, whereas this increase was not observed in iPSC^{lowT}-derived EBs (Fig. 4C, 4D). These changes were reflected in an AA-dependent increase in the percentage of beating iPSC^{highT} and control-derived EBs, but not iPSC^{lowT}-derived EBs (Fig. 4E). These results indicate that AA accelerates and increases CM differentiation of iPSCs with ample telomere reserves, but is unable

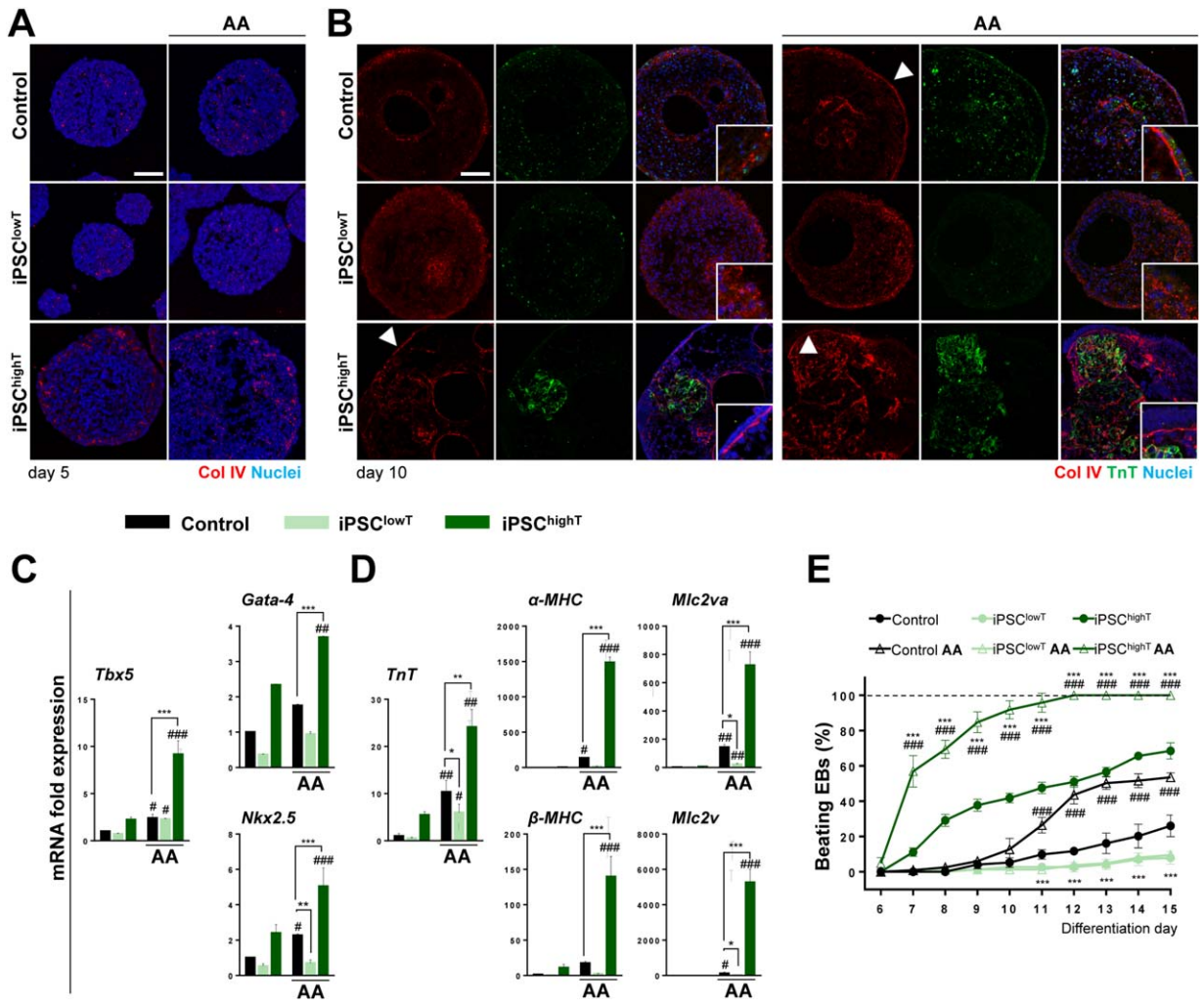

Figure 4. Ascorbic acid supplementation does not support cardiomyocyte differentiation of short-telomere iPSCs. **(A, B)**: Representative images showing collagen IV expression in untreated and ascorbic-acid (AA)-treated day-5 and day-10 EBs. Arrowheads show collagen IV deposition at the BM. Troponin T (TnT) staining shows marked increases in CM numbers after AA treatment in iPSC^{highT}-derived EBs. Scale bar, 80 μm. Inset 40 μm. **(C, D)**: qRT-PCR analysis of (C) cardiac progenitor genes and (D) CM-specific genes, showing AA-stimulated upregulation, especially in iPSC^{highT}-derived EBs. **(E)**: Percentage of beating EBs derived from untreated and AA-treated iPSCs. Data are means ± SEM. * indicates statistical comparison with the control of the same treatment group; # indicates statistical comparison with the corresponding non-AA-treated group. * and #, $p < .05$; ** and ##, $p < .01$; *** and ###, $p \leq .001$. Abbreviations: BM, basement membrane; CMs, cardiomyocytes; EBs, embryoid bodies; iPSCs, induced pluripotent stem cells; TnT, Troponin T.

to drive iPSCs with relatively short telomeres into a CM differentiation program. Thus the selection of iPSC pools with relatively long telomeres combined with AA treatment during differentiation provides a highly-efficient method for obtaining CMs.

Proliferation and Differentiation Capacity of iPSCs with Different Telomere Content Is Determined Cell-Autonomously

The low collagen levels in iPSC^{lowT}-derived EBs, despite AA treatment, suggested that the weak CM differentiation of relatively short-telomere iPSCs might be due to the lack of ECM components. However, seeding of EBs onto the major ECM component collagen IV on differentiation day 5 did not increase the proportion of beating iPSC^{lowT}-derived EBs on day 15 (Supporting Information Fig. S7A). The beating efficiency of iPSC^{lowT}-derived EBs was also unaffected by seeding on matrigel, an artificial ECM mainly composed of growth factors, laminin and collagen IV (Supporting Information Fig. S7A). Lack of CM differentiation was confirmed by assessing CM markers (Supporting Information Fig. S7B). In contrast, seeding of iPSC^{highT}-derived EBs on collagen IV or matrigel increased the proportion of beating EBs on differentiation day 15 to 100% (Supporting Information Fig. S7A).

To test the ability of relatively short-telomere iPSCs to differentiate in a normal microenvironment, we generated chimeric EBs composed of a 1:9-part mix of tdT/iPSC^{lowT} and control iPSCs (chimeric^{lowT}). For comparison, we generated chimeric EBs composed of a 1:9 mix of tdT/iPSC^{highT} and control iPSCs (chimeric^{highT}). iPSCs were first transduced with a lentivirus carrying the tdTomato reporter gene (PGK-tdT) to distinguish the relatively short- and long-telomere subpopulations in chimeric EBs. Since the microenvironment is a well-established source of growth factors [44], we first investigated the proliferation capacity of tdT/iPSC^{lowT} and tdT/iPSC^{highT} in the normal microenvironment of chimeric EBs. Generation of

chimeric EBs did not alter the proportions of tdT/iPSC^{lowT} or tdT/iPSC^{highT} positive for the proliferation marker pH3 (Fig. 5A, 5B). Consistent with the proliferation behavior of iPSC^{highT} and iPSC^{lowT} in non-chimeric EBs, the proportion of tdT/iPSC^{lowT} cells decreased early during chimeric EB differentiation, whereas the proportion of tdT/iPSC^{highT} cells increased (Fig. 5C, 5D). Thus the influence of telomere content on iPSC proliferation capacity is independent of the microenvironment at early stages of in vitro differentiation.

To study the differentiation of tdT/iPSC^{lowT} and tdT/iPSC^{highT} in chimeric EBs, we analyzed the expression of the pluripotent marker Oct3/4. On day 5 after LIF withdrawal, Oct3/4 was present in ~60% of tdT/iPSC^{lowT} from chimeric EBs but was almost absent from tdT/iPSC^{highT} (Fig. 5E, 5F). Such a high percentage of Oct3/4-positive tdT/iPSC^{lowT} cells suggests that a normal microenvironment cannot fix the altered differentiation of iPSCs with relatively short telomeres. Consistent with this finding, most of chimeric^{lowT} EBs were negative for Troponin T, whereas an elevated percentage of chimeric^{highT} EBs were Troponin-T-positive 15 days after LIF withdrawal (Fig. 5G, 5H), indicating that iPSCs with relatively short telomeres barely contribute to the CM pool even in a normal microenvironment. Endoderm identity in tdT/iPSC^{lowT} and tdT/iPSC^{highT} EBs was monitored 15 days after LIF withdrawal by measuring the endodermal marker Sox17. Only 0.97% ± 0.5% of tdT/iPSC^{lowT} differentiated into endoderm in chimeric EBs, whereas the proportion in tdT/iPSC^{highT} EBs was 15.82% ± 4.5% (Supporting Information Fig. S8A, S8B). A normal microenvironment thus does not rescue the inability of short-telomere iPSCs to differentiate into cells of the endodermal lineage.

Ectoderm identity was evaluated by measuring the immature neuron marker Tuj1. The number of tdT, Tuj1 double-positive cells in tdT/iPSC^{lowT} chimeric EBs was more than double that in tdT/iPSC^{highT} chimeric EBs (Supporting Information Fig. S8C, S8D). Consistent with this finding, analysis of non-chimeric EBs revealed higher Tuj-1 protein and RNA expression in iPSC^{lowT}-derived EBs than in iPSC^{highT}-derived EBs (Supporting Information Fig. S8E, S8F). iPSC^{lowT}- and iPSC^{highT}-derived EBs showed even larger expression differences for the neural progenitor marker *Nestin* (Supporting Information Fig. S8G, S8H). Interestingly, this early neuroectodermal gene is also elevated in undifferentiated iPSC^{lowT}, although at a very low level (Supporting information Fig. S8G, S8H). Thus, iPSC^{lowT} do not efficiently differentiate into mesoderm and endoderm but possess an inherent ability to differentiate to the ectoderm lineage.

Discussion

Reprogramming of somatic cells into iPSCs involves net telomere elongation, a requirement for achieving pluripotency status [17, 22, 45–47]. However, little is known about the involvement of telomere length in directing the differentiation fate of telomerase-competent mouse iPSCs. This study demonstrates that cells with relatively long telomeres and high expression of TRF1, a shelterin-complex protein exclusively located at telomeres [48], differentiate more efficiently into CMs than cells with relatively short telomeres and low TRF1 expression. Our results also identify approaches to increasing iPSC telomere content and CM differentiation efficiency.iPSCs show inherent molecular and functional heterogeneity, resulting in differentiation potentials biased toward specific germ lineages [15]. Our chimeric EB experiments demonstrate that fate decisions during early differentiation are determined by cell-intrinsic factors that depend on telomere length. Yet iPSC differentiation fate might also be influence by cell-extrinsic factors [15, 49]. The ECM plays essential roles during heart development and contributes to cell fate determination [42, 50–53]. Two ECM components, collagen IV and fibronectin, facilitate mesoderm induction and CM differentiation [54, 55]. Our results show that the expression levels and organization of collagen IV and fibronectin in EBs depend on the initial iPSC telomere length. Collagen IV and fibronectin are synthesized by endodermal cells [32, 55, 56], and the low expression of these extracellular components might therefore be due to the failure of iPSC^{lowT}-derived EBs to form a complete and organized outer endodermal layer. Moreover, iPSC^{lowT}-derived EBs were unable to differentiate into CMs even in the presence of exogenous collagen IV or matrigel. In contrast, these conditions increased the CM differentiation efficiency of iPSC^{highT} to 100%. Based on these findings, we conclude that cell-autonomous and microenvironmental factors both modulate early differentiation fate of iPSCs differing in telomere length.

Interestingly, the presence of relatively short telomeres impaired mesoderm and endoderm differentiation, but favored ectoderm differentiation. This biased differentiation of iPSC^{lowT} might reflect the fact that the ectodermal lineage is the default differentiation fate of pluripotent cells [57–59]. Differentiation fate is also influenced by EB size, with larger EBs preferentially differentiating to mesoderm and endoderm, while smaller EBs preferentially differentiate to ectoderm [60–66]. Consistent with their small size, iPSC^{lowT}-EBs express high levels of ectoderm markers, whereas the larger iPSC^{highT}-EBs express high levels of endoderm and mesoderm markers. Remarkably, transient increases or decreases in relative telomere length are sufficient to alter the expression patterns of germ layer genes, potentially affecting early differentiation decisions. Regardless of the exact reason for the predisposition of iPSCs with different telomere content to differentiate into different lineages, the results of this study indicate that selecting for telomere content provides a method for determining iPSC fate in vitro.

Differentiation is also altered in ESCs lacking telomerase activity and containing critically short telomeres (*Tert*$^{-/-\ S}$ ESCs) [21]. Similar to our results, the absence of LIF in the culture medium of *Tert*$^{-/-\ S}$ ESCs led to a delayed downregulation of the pluripotent gene *Nanog* when cells were stimulated to differentiate in vitro, in part due to *Dnmt* downregulation [21]. Previous in vivo studies also show that short telomeres negatively affect teratoma formation and chimera production [17, 22, 47, 67]. The present results thus extend previous observations showing the influence of telomere length on the differentiation fate of telomere-competent iPSCs.

The positive correlation between CM differentiation efficiency and telomere length suggests that strategies that increase telomere length in pluripotent cells would augment CM yield. One such strategy is to increase the passage number of iPSCs under proliferation conditions, because telomeres continue to elongate after reprogramming [17]. Supporting

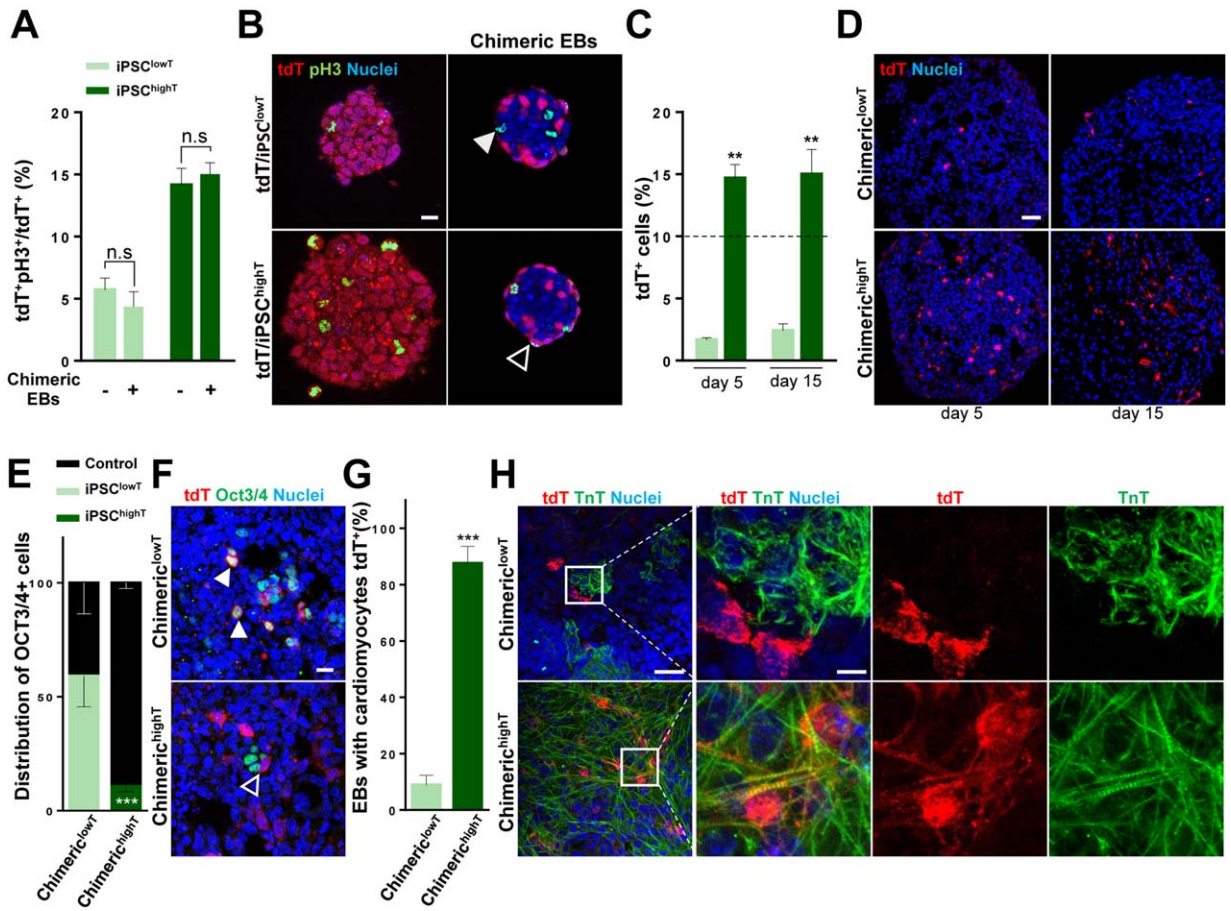

Figure 5. Selecting iPSCs according to telomere content leads to cell-autonomous differences in proliferation and differentiation. **(A)**: pH3-positive cells (%) in 2-day EBs composed of tdT/iPSC^{lowT} only; a 1:9 mix of tdT/iPSC^{lowT} and control iPSCs (chimeric^{lowT} EBs); tdT/iPSC^{highT} only; or a 1:9 mix of tdT/iPSC^{highT} cells and control iPSCs (chimeric^{highT} EBs). **(B)**: Representative immunostaining of tdT (anti-Dsred antibody) and pH3 in non-chimeric and chimeric day-2 EBs. Filled arrowhead highlights non-coexpression of tdT and pH3 in chimeric^{lowT} EBs; unfilled arrowhead marks tdT, pH3^{+} coexpressing cells in a chimeric^{highT} EB. Scale bar, 20 μm. **(C)**: Percentages of tdT/iPSC^{lowT} in chimeric^{lowT} EBs and tdT/iPSC^{highT} in chimeric^{highT} EBs on differentiation days 5 and 15. **(D)**: Representative images of tdT cells in chimeric EBs on the indicated days of differentiation. Scale bar, 40 μm. **(E)**: Quantification of the contribution of tdT/iPSC^{lowT} and tdT/iPSC^{highT} to the overall Oct3/4 population in chimeric EBs. Statistical significance was determined by comparing the proportion of tdT/iPSC^{lowT} Oct3/4^{+} cells with the proportion of tdT/iPSC^{highT} Oct3/4^{+}. **(F)**: Representative immunostaining of Tdt and Oct3/4 in chimeric EBs. Filled arrowheads mark the coexpression of TdT and Oct3/4 preferentially found in chimeric^{lowT} EBs; unfilled arrowhead marks the absence of TdT and Oct3/4 coexpression predominantly found in chimeric^{highT} EBs. Scale bar, 20 μm. **(G)**: Percentage of chimeric EBs with tdT-positive CMs. Only EBs positive for TdT and TnT were included in the analysis. **(H)**: Representative immunostaining of TdT and TnT in chimeric EBs. Magnified views of boxed areas are shown to the right. Scale bars, 40 and 8.5 μm. Bars and values show means ± SEM. All experiments, $n \geq 4$. **, $p < .5$; ***, $p < .001$. Abbreviations: CMs, cardiomyocytes; EBs, embryoid bodies; iPSCs, induced pluripotent stem cells; TnT, Troponin T.

this earlier finding, our results indicate that sorted iPSCs with low telomere content elongate their telomeres in the presence of LIF, resulting in telomere preservation through cell passaging and better CM differentiation efficiency after LIF withdrawal. Therefore, faulty CM differentiation might be restored by exposing iPSCs to a proliferation medium before transfer to differentiation conditions. The differentiation efficiency of iPSC colonies with relatively long telomeres was further increased by treatment with AA. AA promotes CM differentiation by stimulating the proliferation of cardiac progenitors [24], and the lack of an effect in iPSCs with relatively short telomeres could therefore be due to a shortage or abnormal functioning of cardiac progenitors. Our results on the early differentiation of iPSC^{lowT} cells support this idea, revealing sharply reduced expression peaks of cardiac progenitor genes and abnormally elevated expression levels of pluripotency genes. The inability of AA to increase collagen IV expression in iPSC^{lowT} might reflect their faulty differentiation to Sox17-positive cells, since Sox17 activates the transcription of *Col4a1* and *Col4a2* [35]. Moreover iPSC^{lowT} plated onto type IV collagen or matrigel are unable to properly differentiate into CMs, unlike iPSC^{highT}, which all derived-EBs differentiate to CMs under these conditions. These findings, together with the chimera experiments, highlight the importance of selecting iPSCs with relatively long telomeres for obtaining large numbers of CMs.

Conclusion

After a heart attack, ~10^9 CMs are lost [68]. Two main strategies are under investigation to replace this huge number of

CMs: inducing the proliferation of endogenous cardiac cells and grafting exogenous CMs into the injured heart [69, 70]. iPSCs are an important source of exogenous CMs for cell replacement therapy. However, not all iPSC lines differentiate into CMs with the same efficiency [14] and not all have the same telomere length [67]. Our results indicate that the CM differentiation efficiency of iPSCs correlates positively with telomere length. Selection of iPSC lines with ample telomere reserves is thus an attractive strategy for generating large numbers of CMs in a fast, reliable, and efficient way.

Acknowledgments

We thank I. de Diego (CNIC) for technical assistance in EB embedding and sectioning; C. Torroja and F. Sánchez Cabo (CNIC) for help with statistics; the CNIC Cellomic Unit for support in cell sorting and flow cytometry analysis; the CNIC Histology Unit for H&E and pH3 staining and EB paraffin-embedding; the CNIC Viral Vector Unit for PGK-tdTomato production; the CNIC Microscopy Unit for support with image acquisition; the CNIC Animal Facility for mouse care; and S. Bartlett (CNIC) for text editing. The CNIC is supported by the Ministerio de Economia y Competitividad (MINECO) and the Pro-CNIC Foundation, and is a Severo Ochoa Center of Excellence (MINECO award SEV-2015-0505). M.A. Blasco's laboratory was funded by grants from MINECO (SAF2013-45111RETOS), the European Research Council (ERC) Project TEL STEM CELL (GA#232854), the Regional Government of Madrid 2 + 2 ReCaRe, the AXA Research Fund, and the *Fundación Botín*. I. Flores's lab was funded by grants from MINECO (SAF2012-38449) and the Red Temática de Investigación Cooperativa en Enfermedades Cardiovasculares (RD12/0042/0045). E.A. was supported by a FPU predoctoral fellowship from the Ministerio de Educación. T.A. is a postdoctoral fellow supported by the Spanish Association Against Cancer (AECC).

Author Contributions

T.A.: conception and design, collection and assembly of data, data analysis and interpretation, manuscript writing and final approval of manuscript; F.J.G.: collection and assembly of data, data analysis and interpretation, and final approval of manuscript; E.A.: collection and assembly of data, and final approval of manuscript; R.P.S.: provision of study material, and final approval of manuscript; G.G.: data analysis and interpretation, and final approval of manuscript; M.A.B.: provision of study material, and final approval of manuscript; I.F.: conception and design, financial support, provision of study material, data analysis and interpretation, manuscript writing, and final approval of manuscript.

Disclosure of Potential Conflicts of Interest

The authors indicate no potential conflicts of interest.

References

1 Mozaffarian D, Benjamin EJ, Go AS et al. Heart disease and stroke statistics–2015 update: A report from the American Heart Association. Circulation 2015;131:e29–322.
2 von Lueder TG, Krum H. New medical therapies for heart failure. Nat Rev Cardiol 2015;12:730–740.
3 Kikuchi K, Poss KD. Cardiac regenerative capacity and mechanisms. Annu Rev Cell Dev Biol 2012;28:719–741.
4 van Berlo JH, Molkentin JD. An emerging consensus on cardiac regeneration. Nat Med 2014;20:1386–1393.
5 Goumans MJ, Maring JA, Smits AM. A straightforward guide to the basic science behind cardiovascular cell-based therapies. Heart 2014;100:1153–1157.
6 Pavo N, Charwat S, Nyolczas N et al. Cell therapy for human ischemic heart diseases: Critical review and summary of the clinical experiences. J Mol Cell Cardiol 2014; 75:12–24.
7 Hsiao LC, Carr C, Chang KC et al. Stem cell-based therapy for ischemic heart disease. Cell Transplant 2013;22:663–675.
8 Sinnecker D, Goedel A, Laugwitz KL et al. Induced pluripotent stem cell-derived cardiomyocytes: A versatile tool for arrhythmia research. Circ Res 2013;112:961–968.
9 Chong JJ, Murry CE. Cardiac regeneration using pluripotent stem cells–progression to large animal models. Stem Cell Res 2014; 13:654–665.
10 Lalit PA, Hei DJ, Raval AN et al. Induced pluripotent stem cells for post-myocardial infarction repair: Remarkable opportunities and challenges. Circ Res 2014;114:1328–1345.
11 Mummery CL, Lee RT. Is heart regeneration on the right track? Nat Med 2013;19: 412–413.
12 Funakoshi S, Miki K, Takaki T et al. Enhanced engraftment, proliferation, and therapeutic potential in heart using optimized human iPSC-derived cardiomyocytes. Sci Rep 2016;6:19111.
13 Dimmeler S, Ding S, Rando TA et al. Translational strategies and challenges in regenerative medicine. Nat Med 2014;20: 814–821.
14 Kaichi S, Hasegawa K, Takaya T et al. Cell line-dependent differentiation of induced pluripotent stem cells into cardiomyocytes in mice. Cardiovasc Res 2010;88:314–323.
15 Cahan P, Daley GQ. Origins and implications of pluripotent stem cell variability and heterogeneity. Nat Rev Mol Cell Biol 2013; 14:357–368.
16 Chan SW, Blackburn EH. New ways not to make ends meet: Telomerase, DNA damage proteins and heterochromatin. Oncogene 2002;21:553–563.
17 Marion RM, Strati K, Li H et al. Telomeres acquire embryonic stem cell characteristics in induced pluripotent stem cells. Cell Stem Cell 2009;4:141–154.
18 Takahashi K, Tanabe K, Ohnuki M et al. Induction of pluripotent stem cells from adult human fibroblasts by defined factors. Cell 2007;131:861–872.
19 Wang F, Yin Y, Ye X et al. Molecular insights into the heterogeneity of telomere reprogramming in induced pluripotent stem cells. Cell Res 2012;22:757–768.
20 Liu L, Bailey SM, Okuka M et al. Telomere lengthening early in development. Nat Cell Biol 2007;9:1436–1441.
21 Pucci F, Gardano L, Harrington L. Short telomeres in ESCs lead to unstable differentiation. Cell Stem Cell 2013;12:479–486.
22 Schneider RP, Garrobo I, Foronda M et al. TRF1 is a stem cell marker and is essential for the generation of induced pluripotent stem cells. Nat Commun 2013;4: 1946.
23 Maltsev VA, Wobus AM, Rohwedel J et al. Cardiomyocytes differentiated in vitro from embryonic stem cells developmentally express cardiac-specific genes and ionic currents. Circ Res 1994;75:233–244.
24 Cao N, Liu Z, Chen Z et al. Ascorbic acid enhances the cardiac differentiation of induced pluripotent stem cells through promoting the proliferation of cardiac progenitor cells. Cell Res 2012;22:219–236.
25 Flores I, Canela A, Vera E et al. The longest telomeres: A general signature of adult stem cell compartments. Genes Dev 2008;22: 654–667.
26 Layland J, Cave AC, Warren C et al. Protection against endotoxemia-induced contractile dysfunction in mice with cardiac-specific expression of slow skeletal troponin I. FASEB J 2005;19:1137–1139.
27 Rajala K, Pekkanen-Mattila M, Aalto-Setala K. Cardiac differentiation of pluripotent stem cells. Stem Cells Int 2011;2011: 383709.
28 Kathiriya IS, Nora EP, Bruneau BG. Investigating the transcriptional control of cardiovascular development. Circ Res 2015;116: 700–714.

29 Boland MJ, Nazor KL, Loring JF. Epigenetic regulation of pluripotency and differentiation. Circ Res 2014;115:311–324.
30 Valamehr B, Jonas SJ, Polleux J et al. Hydrophobic surfaces for enhanced differentiation of embryonic stem cell-derived embryoid bodies. Proc Natl Acad Sci USA 2008;105:14459–14464.
31 Coucouvanis E, Martin GR. Signals for death and survival: A two-step mechanism for cavitation in the vertebrate embryo. Cell 1995;83:279–287.
32 Li S, Harrison D, Carbonetto S et al. Matrix assembly, regulation, and survival functions of laminin and its receptors in embryonic stem cell differentiation. J Cell Biol 2002;157:1279–1290.
33 Murray P, Edgar D. Regulation of programmed cell death by basement membranes in embryonic development. J Cell Biol 2000;150:1215–1221.
34 Zhang J, Liu G, Ruan Y et al. Dax1 and Nanog act in parallel to stabilize mouse embryonic stem cells and induced pluripotency. Nat Commun 2014;5:5042.
35 Niakan KK, Ji H, Maehr R et al. Sox17 promotes differentiation in mouse embryonic stem cells by directly regulating extraembryonic gene expression and indirectly antagonizing self-renewal. Genes Dev 2010;24:312–326.
36 Kanai-Azuma M, Kanai Y, Gad JM et al. Depletion of definitive gut endoderm in Sox17-null mutant mice. Development 2002;129:2367–2379.
37 Kwon GS, Fraser ST, Eakin GS et al. Tg(Afp-GFP) expression marks primitive and definitive endoderm lineages during mouse development. Dev Dyn 2006;235:2549–2558.
38 Coucouvanis E, Martin GR. BMP signaling plays a role in visceral endoderm differentiation and cavitation in the early mouse embryo. Development 1999;126:535–546.
39 Poschl E, Schlotzer-Schrehardt U, Brachvogel B et al. Collagen IV is essential for basement membrane stability but dispensable for initiation of its assembly during early development. Development 2004;131:1619–1628.
40 Li X, Chen Y, Scheele S et al. Fibroblast growth factor signaling and basement membrane assembly are connected during epithelial morphogenesis of the embryoid body. J Cell Biol 2001;153:811–822.
41 Smyth N, Vatansever HS, Murray P et al. Absence of basement membranes after targeting the LAMC1 gene results in embryonic lethality due to failure of endoderm differentiation. J Cell Biol 1999;144:151–160.
42 Rozario T, DeSimone DW. The extracellular matrix in development and morphogenesis: A dynamic view. Dev Biol 2010;341:126–140.
43 Sato H, Takahashi M, Ise H et al. Collagen synthesis is required for ascorbic acid-enhanced differentiation of mouse embryonic stem cells into cardiomyocytes. Biochem Biophys Res Commun 2006;342:107–112.
44 Discher DE, Mooney DJ, Zandstra PW. Growth factors, matrices, and forces combine and control stem cells. Science 2009;324:1673–1677.
45 Huang Y, Liang P, Liu D et al. Telomere regulation in pluripotent stem cells. Protein Cell 2014;5:194–202.
46 Marion RM, Blasco MA. Telomere rejuvenation during nuclear reprogramming. Curr Opin Genet Dev 2010;20:190–196.
47 Marion RM, Strati K, Li H et al. A p53-mediated DNA damage response limits reprogramming to ensure iPS cell genomic integrity. Nature 2009;460:1149–1153.
48 Garrobo I, Marion RM, Dominguez O et al. Genome-wide analysis of in vivo TRF1 binding to chromatin restricts its location exclusively to telomeric repeats. Cell Cycle 2014;13:3742–3749.
49 Bratt-Leal AM, Carpenedo RL, McDevitt TC. Engineering the embryoid body microenvironment to direct embryonic stem cell differentiation. Biotechnol Prog 2009;25:43–51.
50 Engler AJ, Sen S, Sweeney HL et al. Matrix elasticity directs stem cell lineage specification. Cell 2006;126:677–689.
51 Watt FM, Huck WT. Role of the extracellular matrix in regulating stem cell fate. Nat Rev Mol Cell Biol 2013;14:467–473.
52 Gattazzo F, Urciuolo A, Bonaldo P. Extracellular matrix: A dynamic microenvironment for stem cell niche. Biochim Biophys Acta 2014;1840:2506–2519.
53 Lockhart M, Wirrig E, Phelps A et al. Extracellular matrix and heart development. Birth Defects Res A Clin Mol Teratol 2011;91:535–550.
54 Narazaki G, Uosaki H, Teranishi M et al. Directed and systematic differentiation of cardiovascular cells from mouse induced pluripotent stem cells. Circulation 2008;118:498–506.
55 Cheng P, Andersen P, Hassel D et al. Fibronectin mediates mesendodermal cell fate decisions. Development 2013;140:2587–2596.
56 Li L, Arman E, Ekblom P et al. Distinct GATA6- and laminin-dependent mechanisms regulate endodermal and ectodermal embryonic stem cell fates. Development 2004;131:5277–5286.
57 Turner DA, Trott J, Hayward P et al. An interplay between extracellular signalling and the dynamics of the exit from pluripotency drives cell fate decisions in mouse ES cells. Biol Open 2014;3:614–626.
58 Tropepe V, Hitoshi S, Sirard C et al. Direct neural fate specification from embryonic stem cells: A primitive mammalian neural stem cell stage acquired through a default mechanism. Neuron 2001;30:65–78.
59 Smukler SR, Runciman SB, Xu S et al. Embryonic stem cells assume a primitive neural stem cell fate in the absence of extrinsic influences. J Cell Biol 2006;172:79–90.
60 Park J, Cho CH, Parashurama N et al. Microfabrication-based modulation of embryonic stem cell differentiation. Lab Chip 2007;7:1018–1028.
61 Hwang YS, Chung BG, Ortmann D et al. Microwell-mediated control of embryoid body size regulates embryonic stem cell fate via differential expression of WNT5a and WNT11. Proc Natl Acad Sci USA 2009;106:16978–16983.
62 Lindstrom S, Mori K, Ohashi T et al. A microwell array device with integrated microfluidic components for enhanced single-cell analysis. Electrophoresis 2009;30:4166–4171.
63 Karp JM, Yeh J, Eng G et al. Controlling size, shape and homogeneity of embryoid bodies using poly(ethylene glycol) microwells. Lab Chip 2007;7:786–794.
64 Moon SH, Ju J, Park SJ et al. Optimizing human embryonic stem cells differentiation efficiency by screening size-tunable homogenous embryoid bodies. Biomaterials 2014;35:5987–5997.
65 Burridge PW, Anderson D, Priddle H et al. Improved human embryonic stem cell embryoid body homogeneity and cardiomyocyte differentiation from a novel V-96 plate aggregation system highlights interline variability. Stem Cells 2007;25:929–938.
66 Mohr JC, Zhang J, Azarin SM et al. The microwell control of embryoid body size in order to regulate cardiac differentiation of human embryonic stem cells. Biomaterials 2010;31:1885–1893.
67 Huang J, Wang F, Okuka M et al. Association of telomere length with authentic pluripotency of ES/iPS cells. Cell Res 2011;21:779–792.
68 Laflamme MA, Murry CE. Regenerating the heart. Nat Biotechnol 2005;23:845–856.
69 Sahara M, Santoro F, Chien KR. Programming and reprogramming a human heart cell. EMBO J 2015;34:710–738.
70 Burridge PW, Sharma A, Wu JC. Genetic and epigenetic regulation of human cardiac reprogramming and differentiation in regenerative medicine. Annu Rev Genet 2015;49:461–484.


See www.StemCells.com for supporting information available online.